



SMARCB1 loss induces druggable cyclin D1 deficiency via upregulation of *MIR17HG* in atypical teratoid rhabdoid tumors

Yibo Xue^{1,2†}, Xianbing Zhu^{1,2†}, Brian Meehan³, Sriram Veneti⁴, Daniel Martinez⁵, Geneviève Morin^{1,2}, Rayelle I Maïga^{1,2}, Hongbo Chen⁶, Andreas I Papadakis^{1,2}, Radia M Johnson^{1,2}, Maureen J O'Sullivan^{7,8}, Anat Erdreich-Epstein⁹, Walter H Gotlieb¹⁰, Morag Park^{1,2}, Alexander R Judkins¹¹, Jerry Pelletier^{1,2}, William D Foulkes^{12,13,14} , Janusz Rak³ and Sidong Huang^{1,2*} 

¹ Department of Biochemistry, McGill University, Montreal, Canada

² Goodman Cancer Research Centre, McGill University, Montreal, Canada

³ Department of Pediatrics, McGill University, and Research Institute of McGill University Health Centre, Montreal Children's Hospital, Montreal, Canada

⁴ Pathology and Neuropathology, University of Michigan Medical School, Ann Arbor, MI, USA

⁵ Children's Hospital of Philadelphia Research Institute, Philadelphia, PA, USA

⁶ School of Pharmaceutical Sciences (Shenzhen), Sun Yat-sen University, Guangzhou, PR China

⁷ School of Medicine, University of Dublin, Trinity College, Dublin, Ireland

⁸ Children's Health Ireland at Crumlin, Dublin, Ireland

⁹ Departments of Pediatrics and Pathology, The Saban Research Institute at Children's Hospital Los Angeles and the Norris Comprehensive Cancer Center, University of Southern California, Los Angeles, CA, USA

¹⁰ Division of Gynecologic Oncology, Segal Cancer Center, Jewish General Hospital, McGill University, Montreal, Canada

¹¹ Department of Pathology and Laboratory Medicine, Children's Hospital Los Angeles, Keck School of Medicine of University of Southern California, Los Angeles, CA, USA

¹² Department of Human Genetics, McGill University, Montreal, Canada

¹³ Department of Medical Genetics, Lady Davis Institute, Jewish General Hospital, McGill University, Montreal, Canada

¹⁴ Department of Medical Genetics and Cancer Research Program, McGill University Health Centre, Montreal, Canada

*Correspondence to: S Huang, Department of Biochemistry, McGill University, McIntyre Medical Building, Room 800C, 3655 Promenade Sir William Osler, Montreal, Quebec H3G 1Y6, Canada. E-mail: sidong.huang@mcgill.ca

†These authors contributed equally to this work.

Abstract

Atypical teratoid rhabdoid tumor (ATRT) is a fatal pediatric malignancy of the central neural system lacking effective treatment options. It belongs to the rhabdoid tumor family and is usually caused by biallelic inactivation of *SMARCB1*, encoding a key subunit of SWI/SNF chromatin remodeling complexes. Previous studies proposed that *SMARCB1* loss drives rhabdoid tumor by promoting cell cycle through activating transcription of cyclin D1 while suppressing p16. However, low cyclin D1 protein expression is observed in most ATRT patient tumors. The underlying mechanism and therapeutic implication of this molecular trait remain unknown. Here, we show that *SMARCB1* loss in ATRT leads to the reduction of cyclin D1 expression by upregulating *MIR17HG*, a microRNA (miRNA) cluster known to generate multiple miRNAs targeting *CCND1*. Furthermore, we find that this cyclin D1 deficiency in ATRT results in marked *in vitro* and *in vivo* sensitivity to the CDK4/6 inhibitor palbociclib as a single agent. Our study identifies a novel genetic interaction between *SMARCB1* and *MIR17HG* in regulating cyclin D1 in ATRT and suggests a rationale to treat ATRT patients with FDA-approved CDK4/6 inhibitors.

© 2020 Pathological Society of Great Britain and Ireland. Published by John Wiley & Sons, Ltd.

Keywords: ATRT; cyclin D1; *MIR17HG*; palbociclib; *SMARCB1*

Received 18 February 2020; Revised 27 March 2020; Accepted 10 June 2020

WDF is an Associate Editor of The Journal of Pathology. No other conflicts of interest were declared.

Introduction

SMARCB1-deficient rhabdoid tumors are a family of histologically and genetically related childhood-onset malignancies [1]. While rhabdoid tumors can arise in soft tissues anywhere in the body, they are most frequently found in the central nervous system (CNS),

where they are referred to as atypical teratoid rhabdoid tumors (ATRTs) [1]. Approximately 90% of ATRT cases are diagnosed in children under 3 years of age. Despite current aggressive standard treatments including surgery, radiation therapy, and high-dose chemotherapy with stem cell transplant, most ATRT patients succumb to their disease within 1 year of diagnosis [1,2]. Thus,

identifying druggable vulnerabilities of ATRT is of critical need in order to devise safe and effective treatments.

ATRTs are driven by biallelic inactivating mutations of the tumor-suppressor gene *SMARCB1* (*SNF5*) [3,4], which encodes a key component of SWI/SNF ATP-dependent chromatin remodeling complexes [5,6]. SWI/SNF complexes are polymorphic assemblies of 15 subunits, including a catalytic ATPase subunit, either SMARCA4 or SMARCA2 (BRM), and a variety of associated proteins including SMARCB1 [5,6]. They are known to interact with tissue-specific transcription factors, thus regulating gene expression in a context-dependent manner [5,6].

Similar to ATRT, the closely related non-CNS malignant rhabdoid tumor (MRT), which arises most commonly in the kidney, is also attributed to SMARCB1 loss [3,4]. Gene expression profiling of ATRTs and non-CNS MRTs has shown that they are biologically similar tumors arising in different tissues [7]. However, recent genome-wide profiling studies have revealed distinct subgroups with different genetic and epi-genetic identities within both ATRTs and non-CNS MRTs [8–14], highlighting the complexity of these related tumors.

Forced SMARCB1 expression in an abdomen-derived MRT cell line MON was shown to result in cell cycle arrest by repressing transcription of *CCND1* encoding cyclin D1 [15], which activates CDK4/6, thereby promoting cell cycle progression [16]. Genetic ablation of cyclin D1 in mice that were heterozygous for *Snf5* loss suppressed the formation of rhabdoid tumors [17]. Furthermore, a microarray study showed that brain-derived rhabdoid tumors ($n = 11$) expressed higher levels of *CCND1* compared with normal cerebellum and medulloblastomas [18]. These observations suggest that SMARCB1 loss might drive rhabdoid tumors by upregulating expression of cyclin D1 [6].

However, this SMARCB1-mediated cyclin D1 repression has not been observed in other MRT cell lines such as kidney-derived G401 and muscle-derived A204 [19,20]. Ectopic SMARCB1 expression in A204 cells resulted in upregulation of cyclin D1 protein [19]. Furthermore, *CCND1* expression in 40 extracranial MRTs was significantly reduced when compared with human embryonic stem cells (hESCs) in a recent RNA-seq analysis [9]. Therefore, the relationship between SMARCB1 and cyclin D1 in rhabdoid tumors remains unclear.

We previously undertook an immunohistochemistry (IHC) study of 25 ATRT patient tumors and found that 80% of these tumors showed no evidence of cyclin D1 expression [21]. These findings in this large ATRT collection suggested that SMARCB1 loss may impact cyclin D1 expression through post-transcriptional mechanisms. Indeed, cyclin D1 is frequently dysregulated in cancers and its expression levels can be regulated both transcriptionally and post-transcriptionally [22,23]. Although the protein-level data were clear, the underlying mechanism of cyclin D1 deficiency in ATRT remained to be elucidated.

While SMARCB1 inactivation accounts for 98% of ATRT cases, the other 2% are caused by deleterious

mutations in *SMARCA4* [24]. We and others discovered that biallelic inactivating mutations in *SMARCA4* underlie small cell carcinoma of the ovary, hypercalcaemic type (SCCOHT), a rare and often lethal cancer of young women [25–28]. While SCCOHT and ATRT clearly arise from two distinct organs, they resemble each other at the morphological level including the presence of rhabdoid cells (i.e. cells with eccentric nuclei and abundant eosinophilic cytoplasm) [29,30]. Similar to ATRT, SCCOHT also harbors few other genetic alterations, as indicated by whole-exome sequencing studies [25,26,28]. Furthermore, global DNA methylation analysis in SCCOHT and ATRT suggests that they also share similar epigenomic signatures [31]. We recently uncovered that SMARCA4 directly activates *CCND1* transcription and SMARCA4 loss in SCCOHT and non-small cell lung cancer (NSCLC) results in cyclin D1 deficiency; this leads to exquisite sensitivity to CDK4/6 inhibitors including palbociclib, abemaciclib, and ribociclib [32,33], approved by the US Food and Drug Administration (FDA) for treating a subtype of breast cancer [34–36]. Given the remarkable similarities between ATRT and SCCOHT described above, we postulated that cyclin D1 protein deficiency in ATRT [21] may also result in vulnerability to CDK4/6 inhibition.

In this study, we sought to investigate the underlying mechanisms of cyclin D1 deficiency in ATRT and explored the potential utility of the CDK4/6 inhibitor palbociclib in targeting this lethal cancer affecting infants and young children.

Materials and methods

Cell culture and viral transduction

BT12 and CHLA-266 cell lines were provided by the Children's Oncology Group Cell Culture/Xenograft Repository. CHLA-05, CHLA-02, CHLA-04, and CHLA-06 are low-passage ATRT cell lines developed from pediatric ATRT tumors resected at Children's Hospital Los Angeles (Los Angeles, CA, USA). BT16 was generously donated by Dr PJ Houghton (Nationwide Children's Hospital, Columbus, OH, USA). NHA was from Dr N Jabado (McGill University, Montreal, Quebec, Canada), originally from A Guha (Labatt Brain Tumor Center, Toronto, ON, Canada). All cell lines were maintained at 37 °C in 5% CO₂, and were validated by short tandem repeat (STR) profiling and regularly tested for *Mycoplasma* using a Mycoalert Detection Kit (Lonza, Basel, Switzerland). Details of cell culture can be found in supplementary material, Supplementary materials and methods.

All experiments with ectopic expression and shRNA knockdown were performed using lentiviral transduction following <http://www.broadinstitute.org/rnai/public/resources/protocols>. Infected cells (30 h post-infection) were selected using antibiotics for 2–4 days and harvested immediately for experiments.

siRNA transfection

mirVana® miRNA inhibitor against *miR-19a* (product ID: MH10649) and *miR-17* (product ID: MH12412) were purchased from Thermo Fisher Scientific (Waltham, MA, USA). BT12 and CHLA-06 cells were transfected with these inhibitors at a final concentration of 20 nM using Lipofectamine RNAiMAX (Thermo Fisher Scientific, MA, USA) according to the manufacturer's instructions.

Plasmids

Individual shRNA vectors used were from the Mission TRC library (Sigma, St Louis, MO, USA) provided by the McGill Platform for Cell Perturbation (MPCP): sh*CCND1* #1 (TRCN0000295876), sh*CCND1* #2 (TRCN0000288598), sh*SMARCB1* #1 (TRCN000010503), sh*SMARCB1* #2 (TRCN0000298820). pLX304-*GFP*, pLX304-*CCND1*, pLX317-*GFP*, pLX317-*CDK4*, and pLX317-*SMARCB1* were obtained from TRC3 ORF collections from TransOMIC and Sigma provided by the MPCP. *MIR17HG* was amplified from pcDNA3.1/V5-His-TOPO-mir17-92 [37] and cloned into pPrimer-FF1. The plasmid pcDNA3.1/V5-His-TOPO-mir17-92 was provided by T Duchaine (McGill University) and was originally from Dr JT Mendell, University of Texas Southwestern Medical Center.

Compounds and antibodies

Palbociclib (S1116) was purchased from Selleck Chemicals (Houston, TX, USA). Antibodies against HSP90 (H-114), cyclin D1 (A12), CDK6 (C-21), CDK4 (DCS-35), and p16 (C-20) were from Santa Cruz Biotechnology (Dallas, TX, USA); antibodies against p-RB (S795), PTEN (9188S), and Bim (2933S) were from Cell Signaling Technology (Danvers, MA, USA); and antibody against SMARCB1 (A301-087A) was from Bethyl Laboratories (Montgomery, TX, USA). Antibody against Rb (554136) was from BD Pharmingen (San José, CA, USA). Antibodies used for immunohistochemistry are listed in Supplementary materials and methods.

Immunohistochemistry of patient tumor samples and automated quantification

Three TMAs used were previously described: 36 ATRTs [21], 59 HGSCs, and 32 SCCOHTs [33]. Studies were approved by the Institutional Review Board (IRB) of Children's Hospital of Philadelphia (ATRt), Jewish General Hospital (HGSC), and McGill University (SCCOHT). ATRT samples were obtained retrospectively from archival pathology material from deceased patients (no informed consent was obtained) after IRB approval, with all identifiers removed. Informed consent was obtained from all HGSC and SCCOHT participants. Details are given in supplementary material, Supplementary materials and methods.

Colony formation assays

Since different cell lines have variable proliferation rates and sizes, plating densities were first optimized to allow

~2 weeks of drug treatment, before reaching 90% confluency. Single cell suspensions were then counted and seeded into six-well plates with optimized densities ($2-8 \times 10^4$ cells per well). Cells were treated with vehicle control or drugs on the following day and culture medium was refreshed every 3 days. At assay endpoints, cells were fixed with 3.75% formaldehyde, stained with crystal violet (0.1% w/v), and photographed. All relevant assays were performed independently at least three times.

Cell viability assays

Cells were seeded into 96-well plates (1000–2000 cells per well). Twenty-four hours after seeding, CDK4/6 inhibitors were added to final drug concentrations ranging from 0.0026 to 10 μ M. Cells were then incubated for 5–7 days and viability was measured using the CellTiter-Blue assay (Promega, Madison, WI, USA). Relative survival of treated cells was normalized to the untreated controls after background subtraction.

Protein lysate preparation and immunoblots

Cells were first seeded in normal medium without drug. The medium was replaced the next day with or without drug as indicated. After drug stimulation, cells were washed with cold PBS, lysed with protein sample buffer, and processed with Novex® NuPAGE® Gel Electrophoresis Systems (Thermo Fisher Scientific, MA, USA).

RNA isolation and RT-qPCR

Cells seeded a day before were harvested for RNA isolation using Trizol (Thermo Fisher Scientific, MA, USA). Synthesis of cDNAs using the Maxima First Strand cDNA Synthesis Kit (Thermo Fisher Scientific, MA, USA) and RT-qPCR assays using SYBR® Green master mix (Roche) or Taqman probes for miRNAs (Thermo Fisher Scientific, MA, USA) were performed according to the manufacturers' protocols. Relative mRNA levels of each gene shown were normalized to the expression of the house keeping gene *GAPDH*. Details of the sequences of the primers are listed in supplementary material, Supplementary materials and methods.

Cell line RNA-seq

Total RNA from cell lines was extracted with an RNeasy Mini Kit (Qiagen, Hilden, Germany) and quality controlled and subjected to RNA-seq at Genome Quebec (Montreal, Quebec, Canada). Data analysis was performed as previously described [33]. Details are given in supplementary material, Supplementary materials and methods.

Chromatin immunoprecipitation (ChIP)

Sixty million BT12 cells were fixed in complete media containing 0.3% formaldehyde for 30 min at 4 °C and then quenched with 0.125 M glycine for 5 min. Fixed cells were pelleted and washed twice with PBS before

snap-freezing on dry ice. Antibody against SMARCB1 (Abcam, Cambridge, UK; 12167) was used for ChIP experiments by following a protocol using MNase [38]. The sequences of the primers used for RT-qPCR assays are listed in supplementary material, Supplementary materials and methods.

Mouse intracranial tumor model and *in vivo* drug studies

All procedures involving animals were performed in accordance with the guidelines of the Canadian Council of Animal Care and the Animal Utilization Protocols, approved by the Institutional Animal Care Committee at McGill University Health Centre Research Institute and McGill University.

The ATRT-derived cell line CHLA-06, expressing firefly luciferase, was used to generate intracranial orthotopic tumors in *scid/IL2Rg^{null}* mice (NSG, 005557; NOD-*scid/IL2Rg^{null}*; NSG; Jackson Laboratories, Bar Harbor, ME, USA) essentially as described previously [39]. Mice were also imaged twice per week using an IVIS 200 Imager (Perkin Elmer, Waltham, MA, USA) after intraperitoneal injection of 150 mg/kg of D-luciferin (firefly, potassium salt; Caliper Life Sciences, Waltham, MA, USA). Mice received palbociclib, 150 mg/kg per day or placebo/vehicle (50 mM sodium L-lactate buffer, pH 4.0) in the 200 μ l volume administered by oral gavage. Details may be found in supplementary material, Supplementary materials and methods.

Statistical analyses

Statistical significance was calculated using two-tailed Student's *t*-tests, two-way ANOVA or non-parametric Mann-Whitney tests. Prism software (GraphPad Inc, San Diego, CA, USA) was used to generate graphs and statistical analyses. Error bars show standard deviation (SD) or standard error of the mean (SEM). **p* < 0.05, ***p* < 0.01, ****p* < 0.001, *****p* < 0.0001.

Results

Cyclin D1 deficiency in ATRT is caused by SMARCB1 loss

Our previous IHC study of 25 SMARCB1-deficient ATRT patient tumors found that 80% of these cases showed absence of cyclin D1 protein expression [21]. To further confirm this finding, we employed unbiased automated quantification [40] to re-analyze published IHC data of 25 AT/RT samples [21] and ten additional unpublished cases (*n* = 35), along with ovarian high-grade serious carcinomas (HGSCs; *n* = 52) and SCCOHT tumors (*n* = 32), which served as positive and negative staining controls, respectively, due to their known cyclin D1 status [33]. Identical IHC antibody and protocols were used for all tumors to allow direct comparison. Similar to SCCOHTs, cyclin D1 IHC signal

was negative in most ATRTs (Figure 1A,B). Furthermore, ATRTs were generally RB-proficient and p16-deficient, which resembles SCCOHTs and is the reverse of HGSCs (Figure 1A,B). The p16 deficiency in ATRT is consistent with previous studies showing that SMARCB1 activates *CDKN2A* transcription [41]. These data confirm and extend our previous findings of cyclin D1 protein deficiency in ATRT [21].

Recent studies classified ATRT into three subtypes (TYR, SHH, and MYC) based on DNA methylation and gene expression profiling [10,12–14]. We analyzed the cyclin D1 protein expression in a panel of ATRT cell lines (BT12, CHLA-226, CHLA-06, CHLA-05, CHLA-02, CHLA-04, and BT16), representing different ATRT subtypes as defined by recent studies. Consistent with our above observations in patient-derived tumors, western blot analysis showed that these ATRT cell lines expressed lower levels of cyclin D1 and p16 protein compared with NHA, a non-transformed human astrocyte cell line (Figure 1C). Since recent studies suggest that ATRT subtypes may originate from different precursor cells [8,10–13], NHA may not be the perfect control for all subtypes. Therefore, it was important to compare cyclin D1 expression in isogenic ATRT cell pairs engineered to differ only in SMARCB1 status. Similar to previous studies in non-CNS MRT cells [15,19,42], SMARCB1 restoration in all ATRT cell lines tested (BT12, CHLA-226, CHLA-06, CHLA-02, and BT16) resulted in strong growth inhibition (supplementary material, Figure S1) and elevated p16 expression (Figure 1D). However, cyclin D1 expression was strongly elevated in these SMARCB1-restored ATRT cell lines (Figure 1D). Complementary to these findings, knockdown of *SMARCB1* in NHA cells using two independent shRNAs strongly suppressed cyclin D1 expression (Figure 1E). Together, these data suggest that SMARCB1 loss in ATRT reduces cyclin D1 protein expression.

SMARCB1 suppresses *MIR17HG* expression in ATRT

SMARCA4 loss leads to strong downregulation of *CCND1* transcription through impacting the chromatin structure at its gene locus in both SCCOHT and NSCLC [32,33]. Considering the similarities between SCCOHT and ATRT [30], we investigated whether this potential mechanism is operative in cyclin D1 regulation by SMARCB1 in ATRT. In contrast to SCCOHT and NSCLC, SMARCB1 restoration only resulted in a mild upregulation (~1.5- to 2-fold) of *CCND1* mRNA expression (supplementary material, Figure S2), suggesting additional post-transcriptional regulation. To uncover the underlying mechanism, we performed transcriptome analysis of two commonly used ATRT cell lines, CHLA-06 (suspension) and BT12 (adhesive), with or without SMARCB1 restoration using RNA sequencing (RNA-seq). We identified 632 upregulated and 158 downregulated common genes as a result of SMARCB1 restoration in both cell line pairs (Figure 2A and supplementary material, Table S1). This

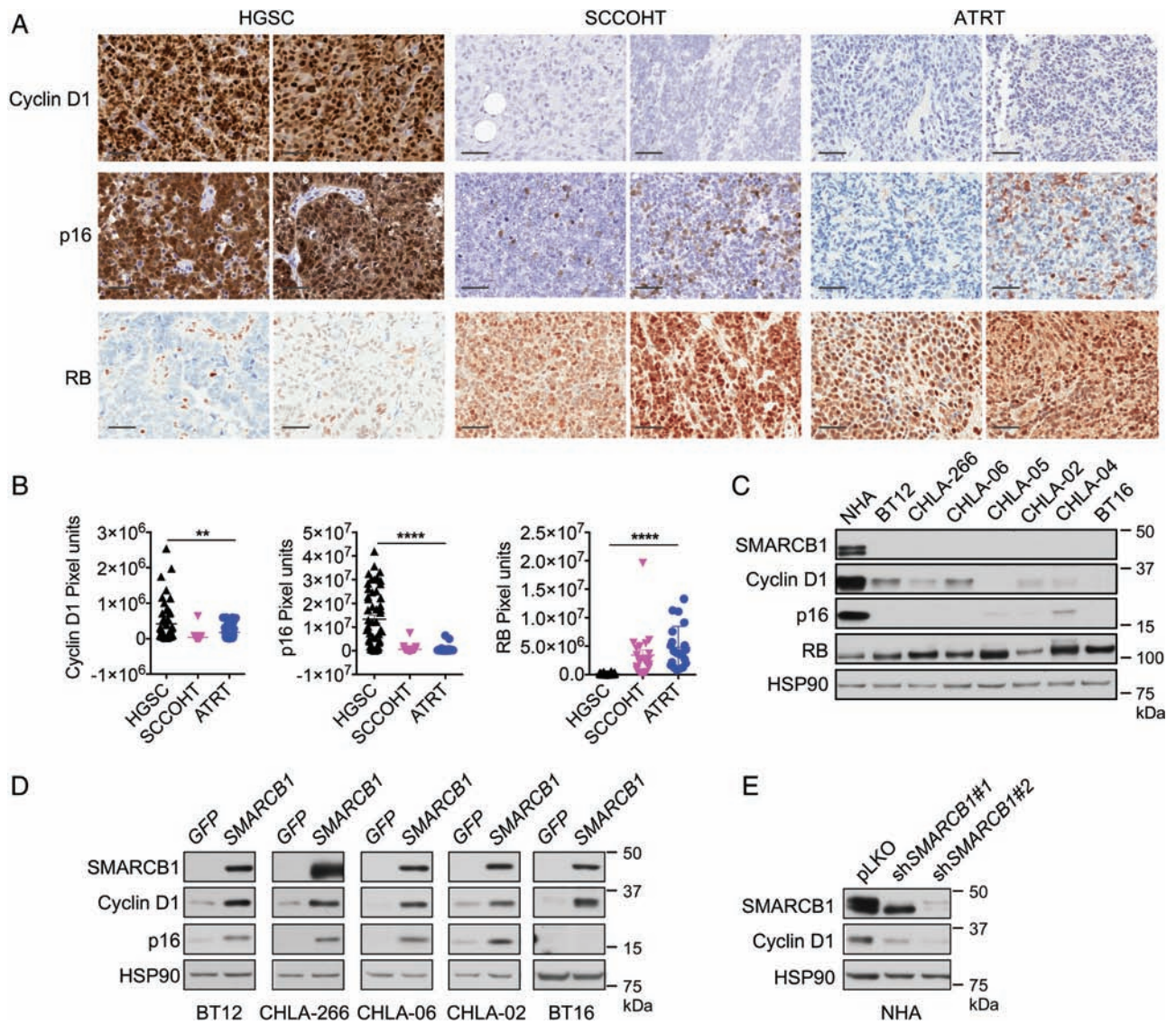


Figure 1. SMARCB1 loss leads to cyclin D1 deficiency in ATRT. (A, B) ATRT patient tumors express low levels of cyclin D1 and retain the RB-proficient/p16-deficient profile. Immunohistochemistry (IHC) analysis coupled with unbiased automated quantification [40] was performed on high-grade serous carcinomas (HGSC; $n = 52$), SCCOHT ($n = 32$), and ATRT ($n = 35$) patient tumors for the expression of cyclin D1, p16, and RB. Representative images of the IHC analysis (A) and quantification results (B) are shown. Bar = 50 μm ; non-parametric Mann–Whitney test, ** $p < 0.01$, **** $p < 0.0001$; ns, not significant. Error bars show SEM. (C) Western blot analysis of indicated proteins in a panel of NHA and seven ATRT cell lines. (D) Expression of cyclin D1 and p16 in indicated ATRT cell lines with or without SMARCB1 restoration. (E) Expression of cyclin D1 in NHA cells with or without expression of shRNAs targeting SMARCB1. HSP90 served as a loading control.

is consistent with the role of SWI/SNF complex, which can function as both a transcription activator and a suppressor [43]. To help identify the potential direct targets of SMARCB1 among these candidates, we compared this list with genes whose loci showed SMARCB1 occupancy within 100 kbp from their transcription start sites from a published chromatin immunoprecipitation sequencing (ChIP-seq) study in SMARCB1-proficient HeLa cells [44]. We rationalized that this endogenous SMARCB1 ChIP-seq study in HeLa cells may help to identify SMARCB1 target genes conserved among different cell types. This analysis identified 20 candidate genes, of which 11 were upregulated and nine were downregulated upon SMARCB1 restoration in ATRT cells (Figure 2B).

Among these candidates, *MIR17HG* is particularly interesting as it has been previously linked to post-transcriptional regulation of cyclin D1, which may explain our above observations in ATRT (Figure 1). *MIR17HG* encodes a cluster of six miRNAs (*miR-17-92*), three of which (*miR-19a*, *miR-17*, and *miR-20a*) have been shown to target cyclin D1 [45–48]. miRNAs are small non-coding RNAs of 20–22 nucleotides that inhibit gene expression by repressing translation but also accelerating mRNA degradation [49]. Verifying our RNA-seq results, RT-qPCR analysis showed that *MIR17HG* is significantly suppressed upon SMARCB1 restoration in BT12 and CHLA-06 cells (Figure 2C). Additional published ChIP-seq data sets also showed an enrichment of SMARCB1 occupancy in the

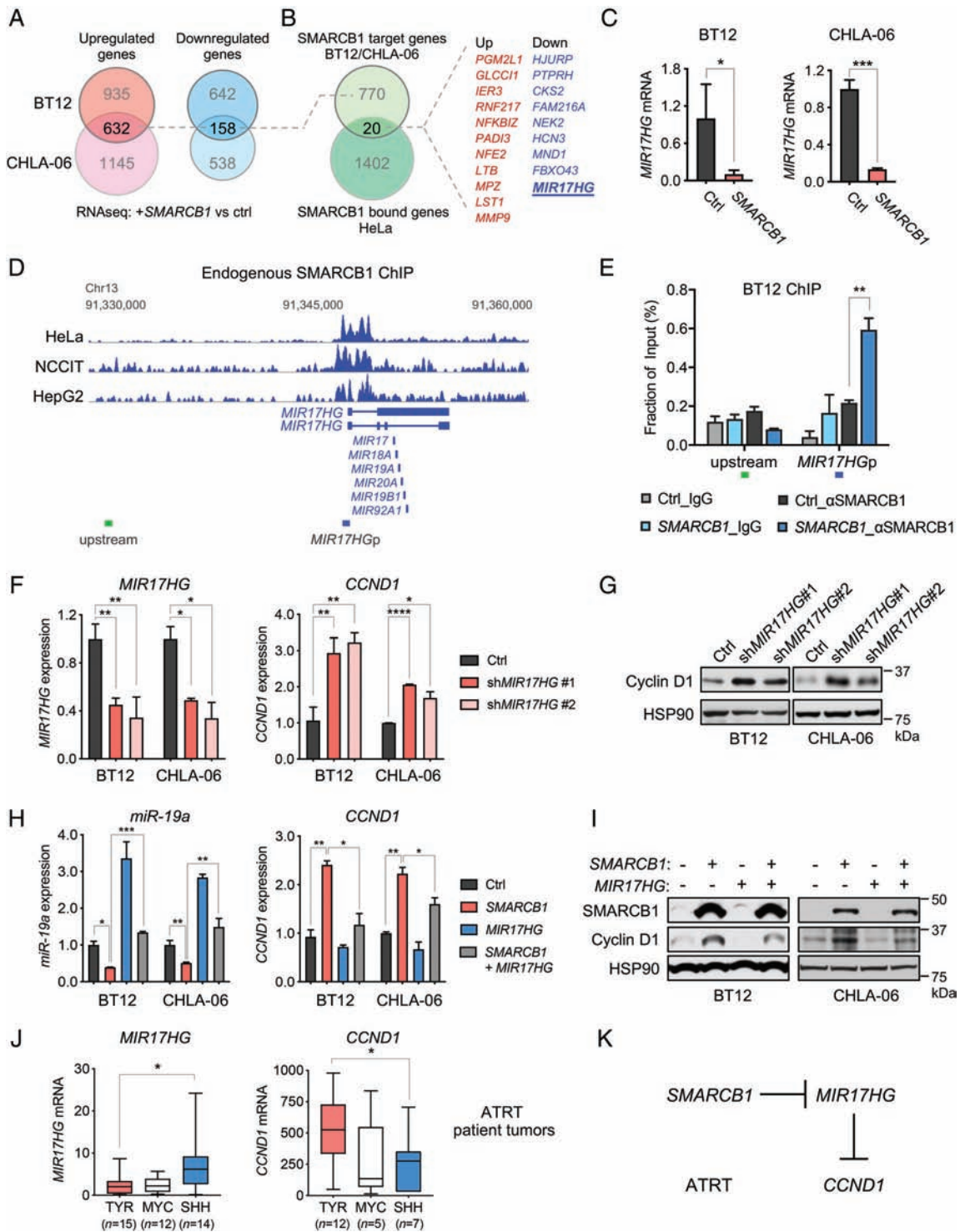


Figure 2. *MIR17HG* contributes to *SMARCB1*-mediated cyclin D1 regulation in ATRT. (A) Venn diagrams of the number of genes upregulated or downregulated in RNA-seq analysis with BT12 and CHLA-06 upon *SMARCB1* restoration ($n = 3$, fold-change > 2.5 , adjusted $p < 0.01$). (B) Overlapping genes in *SMARCB1* common regulated genes from RNA-seq data in ATRT cells and genes that showed *SMARCB1* occupancy within 100 kbp from their TSS in *SMARCB1*-proficient HeLa cells from a previous study [50]. Red-labeled genes are upregulated and blue are downregulated. (C) RT-qPCR analysis of *MIR17HG* mRNA in BT12 and CHLA-06 cells with or without *SMARCB1* restoration. (D) ChIP-seq data in vicinities of the *MIR17HG* locus indicate enhanced *SMARCB1* binding at promoter regions in indicated cell lines. (E) *SMARCB1* ChIP-PCR for regions at *MIR17HG* promoter and upstream control site in BT12 cells with or without *SMARCB1* restoration. Locations of these two sites are indicated as blue and green bars in D. IgG served as an antibody control. (F) RT-qPCR analysis of *MIR17HG* and *CCND1* in BT12 and CHLA-06 cells expressing shRNAs targeting *MIR17HG*. (G) Cyclin D1 protein expression in BT12 and CHLA-06 cells expressing shRNAs targeting *MIR17HG*. (H) RT-qPCR analysis of *miR-19a* and *CCND1* expression in BT12 and CHLA-06 cells expressing *SMARCB1* or/and *MIR17HG*. *miR-19a* is a mature miRNA generated from *MIR17HG*. *miR-19a* expression was normalized to *U6*, and *CCND1* mRNA was normalized to *GAPDH*. (I) Cyclin D1 protein expression in BT12 and CHLA-06 cells expressing *SMARCB1* or/and *MIR17HG*. HSP90 served as a loading control in western blot results. (J) Expression of *CCND1* and *MIR17HG* mRNA in indicated subtypes of ATRT patient tumors from a published microarray study [10]. (K) Schematic diagram for *MIR17HG*-mediated cyclin D1 regulation by *SMARCB1* in ATRT. Two-tailed t -test. Error bars show SD; * $p < 0.05$, ** $p < 0.01$, *** $p < 0.001$.

promoter region of *MIR17HG* in NCCIT and HepG2 cells (Figure 2D) [50–52]. In SMARCB1-restored BT12 cells, our ChIP-PCR detected significant SMARCB1 occupancy at the *MIR17HG* promoter but not at an upstream region of the *MIR17HG* locus (Figure 2E). Together, these data indicate that SMARCB1 loss activates *MIR17HG* by directly interacting with its gene locus, which may contribute to the reduced cyclin D1 expression in ATRT cells.

MIR17HG contributes to cyclin D1 deficiency induced by SMARCB1 loss in ATRT

To evaluate the role of *MIR17HG* in regulating cyclin D1 expression, we knocked down *MIR17HG* with two independent shRNAs in three ATRT cell lines, BT12, CHLA-06, and BT16 (Figure 2F and supplementary material, Figure S3A). Cyclin D1 was upregulated at both mRNA and protein levels in all cell lines (Figure 2F,G and supplementary material, Figure S3B, C), mirroring the role of miRNAs in inducing mRNA degradation and inhibiting translation [49]. While it is possible that any of the six miRNAs encoded by *MIR17HG* may contribute to cyclin D1 regulation, we focused on *miR-17* and *miR-19a*, which have been shown to target *CCND1* mRNA [45–48]. As expected, their inhibition led to elevation of *cyclin D1* mRNA and protein expression in BT12 and CHLA-06 cells (supplementary material, Figure S4). However, *MIR17HG* suppression had little effect on the expression of PTEN and BIM, known targets of this miRNA cluster characterized in other cancers [53,54] (supplementary material, Figure S5), likely due to context dependency of miRNA regulation [55]. Nevertheless, these data confirmed that *MIR17HG* plays a key role in determining cyclin D1 expression in ATRT.

To investigate the contribution of *MIR17HG* to SMARCB1-mediated cyclin D1 regulation, we performed rescue experiments where *MIR17HG* was ectopically expressed in ATRT cells with or without SMARCB1 restoration. The expression of mature *miR-19a*, known to target cyclin D1 in several other contexts [46,48], was measured as a read-out for effective processing of exogenous *MIR17HG*. In line with Figure 2C, SMARCB1 restoration suppressed *miR-19a* in both BT12 and CHLA-06 cells (Figure 2H). Ectopic expression of *MIR17HG* in SMARCB1-restored ATRT cells led to an expected increase in *miR-19a* expression and contaminant suppression of SMARCB1-induced cyclin D1 upregulation, at both mRNA and protein levels (Figure 2H,I). Supporting this *MIR17HG*-mediated regulation of cyclin D1 in ATRT, *CCND1* mRNA tends to be inversely correlated with *MIR17HG* expression in our cell line panel (supplementary material, Figure S6). Furthermore, in a previous study classifying ATRT patient tumors into three subtypes (TYR, MYC, and SHH) [10], we observed an inverse association between *MIR17HG* and *CCND1* mRNA expression among these subtypes (Figure 2J). Collectively, these data suggest that SMARCB1 loss results in cyclin D1 deficiency in

ATRT at least in part through elevating *MIR17HG* expression (Figure 2K).

Cyclin D1 deficiency causes sensitivity of ATRT to CDK4/6 inhibition both *in vitro* and *in vivo*

We recently showed that cyclin D1 deficiency induced by SMARCA4 loss constrains CDK4/6 kinase activity, which leads to susceptibility to CDK4/6 inhibition in multiple cancer types [32,33]. Given that ATRT is also deficient in cyclin D1 protein expression via a different mechanism, we investigated the drug sensitivities of ATRT to CDK4/6 inhibition. While pan-CDK inhibitor showed efficacy in targeting MRT [56,57], highly selective CDK4/6 inhibitors such as palbociclib have not been evaluated as single agents to target ATRT. We found that ATRT cells, but not NHA controls, are highly sensitive to palbociclib in both long-term colony formation and short-term cell viability assays (Figure 3A,B). Consistently, phosphorylation of RB, a direct target of CDK4/6, was significantly inhibited in ATRT cells but not in NHA cells (Figure 3C). To evaluate the efficacy of palbociclib in treating ATRT *in vivo*, we generated an orthotopic mouse model where CHLA-06 cells (labeled with luciferase for visualizing tumor burden in live animals) were intracranially engrafted into brains of immunodeficient mice. As shown in Figure 3D,E, palbociclib treatment of established tumors resulted in potent inhibition of tumor-related bioluminescence, indicating a strong therapeutic response for palbociclib as a single agent.

To investigate the contribution of cyclin D1 deficiency to palbociclib response in ATRT, we ectopically overexpressed cyclin D1 in two ATRT cell lines, CHLA-06 and BT12. As shown in Figure 3F–I, cyclin D1 ectopic expression increased RB phosphorylation and conferred substantial resistance to palbociclib in both cell lines. In contrast, overexpression of the target of palbociclib, CDK4, did not confer resistance, suggesting that cyclin D1 is the rate-limiting factor. In keeping with this, knockdown of cyclin D1 in BT12, which expresses higher levels of cyclin D1 compared with other ATRT cell lines (Figure 1C), further sensitized these cells to palbociclib treatment (Figure 3J,K). This is consistent with our previous findings in SMARCA4-deficient cancers [32,33]. Taken together, these data demonstrate that cyclin D1 deficiency induced by SMARCB1 loss is a key determinant of palbociclib sensitivity in ATRT.

Discussion

Our study demonstrates that cyclin D1 protein deficiency in ATRT is caused by SMARCB1 loss at least in part through upregulation of *MIR17HG*, which is known to produce mature miRNAs targeting cyclin D1. Furthermore, we establish that this cyclin D1 deficiency in ATRT cells contributes to their susceptibilities to CDK4/6 inhibition.

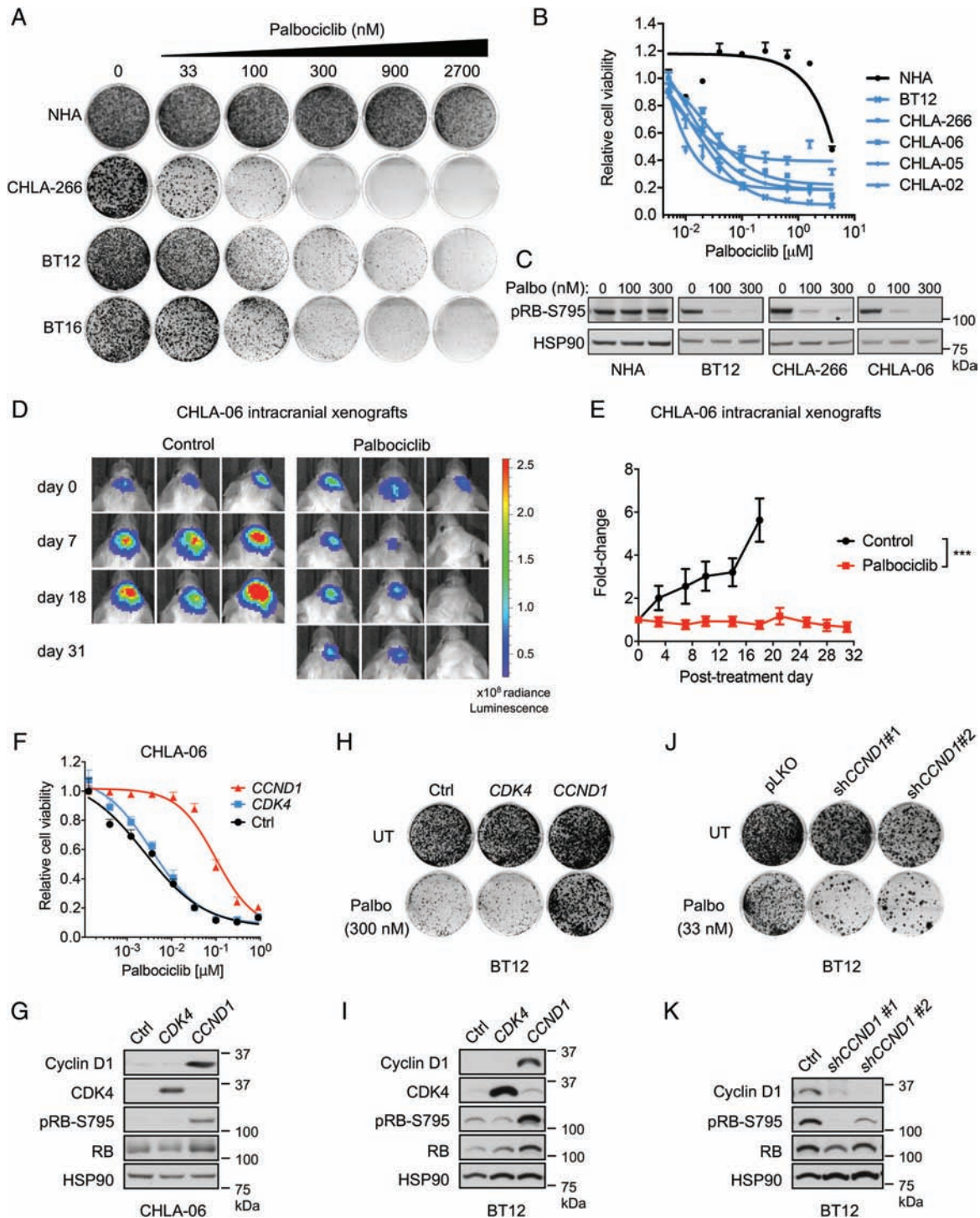


Figure 3. Cyclin D1 deficiency underlies sensitivity to CDK4/6 inhibition in ATRT. (A) Colony formation assay of NHA control or ATRT (BT12 and CHLA-266) cells cultured in the absence or presence of palbociclib for 10–14 days. (B) Cell viability assay of ATRT cells (BT12, CHLA-266, CHLA-06, CHLA-05) and NHA. Cells were treated with palbociclib for 6 days and subjected to a CellTiter-Blue assay. (C) Levels of pRB-S795 in cells treated with palbociclib at 0, 100 or 300 nM for 24 h were analyzed by western blotting. HSP90 served as a loading control. (D, E) Efficiency of palbociclib in suppressing tumor growth in an orthotropic mouse model of ATRT. CHLA-06 cells expressing pLX317-Luciferase were intracranially engrafted into brains of NSG mice. After tumor establishment, mice were treated with vehicle for up to 18 days (reached endpoint due to tumor burden) or palbociclib (150 mg/kg) for 31 days. Tumor burden in live animals was visualized using an *in vivo* imaging system. Tumor-related luminescence images of representative mice (D) and luminescence fold-change over time (E) of all animals (control, $n = 4$; palbociclib-treated, $n = 6$; two-way ANOVA, $***p < 0.001$) are shown. Radiance ($p/s/cm^2/sr$), color scale (minimum = 2.6×10^7 ; maximum = 2.6×10^8). (F, H) Cell viability assay of CHLA-06 cells (F) and colony formation assay of BT12 cells (H) stably expressing control vector, *CDK4* or *CCND1* treated with indicated concentration of palbociclib. (G, I) Levels of pRB-S795, CDK4, and cyclin D1 were determined by western blot. (J) Colony formation assay of BT12 cells expressing shRNAs targeting cyclin D1 treated with palbociclib at 33 nM. (K) Levels of pRB-S795 and cyclin D1 were determined by western blot. HSP90 served as a loading control.

Previous data show that ATRT and SCCOHT are both driven by biallelic inactivation of one of the key SWI/SNF components. As described in the Introduction, these two cancers, while arising from two distinct organs, closely resemble each other at the histopathological, genetic, and epigenetic levels [30]. Furthermore, both cancers exhibit cyclin D1 deficiency caused by their driver mutations. In SCCOHT, this is at the level of direct transcriptional regulation – SMARCA4 loss results in strong suppression of *CCDN1* expression [33]. In ATRT, SMARCB1 loss causes altered post-transcriptional regulation of cyclin D1 mediated by *MIR17HG*. Similar to SCCOHT, ATRT cells are also highly sensitive to CDK4/6 inhibition due to their cyclin D1 deficiency, supporting the notion whereby critically low oncogene levels, caused by loss of a driver tumor suppressor, may also be exploited therapeutically.

In addition to *MIR17HG*, other SMARCB1 target genes may also contribute to the cyclin D1 dysregulation in ATRT. We also recognize that this cyclin D1 deficiency likely does not promote cell cycle progression and drive these cancers and may be compensated by other cell cycle regulators, which remains to be investigated. miRNAs encoded by *MIR17HG* are known to be oncogenic, with expression frequently upregulated in cancers [58]. Thus, it is possible that *MIR17HG* upregulation by SMARCB1 loss independently contributes to the development of ATRT. Since the best-characterized tumor suppressor targets PTEN and BIM are not regulated by *MIR17HG* in ATRT cells, the role of *MIR17HG* in ATRT tumorigenesis needs further studies.

Our data suggest that ATRT tumors may be responsive to CDK4/6 inhibitors as single agents due to their deficiency in (and hence heightened dependence on) cyclin D1 expression. Furthermore, we show that ATRT patient tumors were generally RB-proficient and p16-deficient, a known profile associated with positive responses to CDK4/6 inhibitors [34–36]. It has been shown that pan-CDK inhibitors have promising efficiencies in targeting ATRT in preclinical studies [56,57], although with the rationale that these tumors have activated cyclin D1 caused by SMARCB1 loss based on previous studies in MRT. Independently supporting our model, overexpression of cyclin D1 has been observed in rhabdoid tumor resistant to pan-CDK inhibitor in mouse [56]. In addition, a recent phase I dose-escalation study in 13 ATRT patients showed that the two patients who received more than four cycles (3 weeks on/1 week off) of ribociclib (another FDA-approved CDK4/6 inhibitor similar to palbociclib) treatment achieved stable disease and remained stable on treatment for more than 20 months of follow-up [59]. Considering that all patients enrolled had progressed on previous standard therapy and the other 11 patients only received one or two cycles of ribociclib [59], these results support the anti-tumor activities of CDK4/6 inhibitors in ATRT patients.

It is also important to identify biomarkers of drug responses to improve the potential clinical utility of CDK4/6 inhibitors in treating ATRT. Our *in vitro* data suggest that cyclin D1 expression itself may be a potential biomarker – forced cyclin D1 overexpression in ATRT cells resulted in resistance to palbociclib. While our IHC results indicate an overall cyclin D1 deficiency in ATRT patient tumors, variable cyclin D1 expression was observed among these cases. This could potentially be due to the differential cyclin D1 expression in ATRT subtypes [10,13,14], which may be determined by a different cell-of-origin in brain and/or the age of patients of these subgroups [13]. This warrants further investigations. In addition, combination of CDK4/6 inhibition with other approaches showing efficacies in ATRT such as high-dose chemotherapy and focal radiation [60] may also be explored. Indeed, it has been shown that palbociclib enhances radiation therapy effects in ATRT models [61].

In summary, our study reveals an underlying mechanism for cyclin D1 deficiency in ATRT patient tumors, linking SMARCB1 to *MIR17HG* in regulating cyclin D1. Furthermore, our data suggest that this vulnerability of ATRT can be exploited therapeutically using the FDA-approved CDK4/6 inhibitors to improve the survival of children affected by this fatal disease.

Acknowledgements

We thank Dr Thomas Duchaine for sharing the pcDNA3.1/V5-His-TOPO-mir17-92 plasmid for cloning. This work was supported by Canadian Institutes of Health Research (CIHR) grants MOP-130540 and PJT-156233 (SH), FDN-148390 (WDF), and FDN 143322 (JR). YX is supported by a Rolande & Marcel Gosselin Graduate Studentship and Charlotte & Leo Karassik Foundation Oncology PhD Fellowship. SH is supported by a Canadian Research Chair in Functional Genomics. JR is supported by the Jack Cole Chair in Pediatric Hematology/Oncology.

Author contributions statement

YX, XZ, BM, GM, HC, AIP and RIM performed experiments. RMJ conducted bioinformatics analysis. SV, DM and ARJ provided pathology expertise. MO'S, AEE and WHG provided reagents and advice. MP, JP, WDF, JR and SH supervised the experiments. YX, WDF and SH wrote the manuscript. SH oversaw the study. All the authors read and approved the final manuscript.

Data availability statement

The RNA-seq data have been deposited in the Gene Expression Omnibus (GEO) under the access number

GSE147851 (<https://www.ncbi.nlm.nih.gov/geo/query/acc.cgi?acc=GSE147851>).

All other data are contained within this article and supporting data will be available by contacting the corresponding author.

References

- Margol AS, Judkins AR. Pathology and diagnosis of SMARCB1-deficient tumors. *Cancer Genet* 2014; **207**: 358–364.
- Chi SN, Zimmerman MA, Yao X, et al. Intensive multimodality treatment for children with newly diagnosed CNS atypical teratoid rhabdoid tumor. *J Clin Oncol* 2009; **27**: 385–389.
- Verstege I, Sevenet N, Lange J, et al. Truncating mutations of hSNF5/INI1 in aggressive paediatric cancer. *Nature* 1998; **394**: 203–206.
- Biegel JA, Zhou JY, Rorke LB, et al. Germ-line and acquired mutations of *INI1* in atypical teratoid and rhabdoid tumors. *Cancer Res* 1999; **59**: 74–79.
- Kadoch C, Crabtree GR. Mammalian SWI/SNF chromatin remodeling complexes and cancer: mechanistic insights gained from human genomics. *Sci Adv* 2015; **1**: e1500447.
- Wilson BG, Roberts CW. SWI/SNF nucleosome remodellers and cancer. *Nat Rev Cancer* 2011; **11**: 481–492.
- Gruppenmacher AT, Halpern AL, Bonaldo MF, et al. Study of the gene expression and microRNA expression profiles of malignant rhabdoid tumors originated in the brain (AT/RT) and in the kidney (RTK). *Childs Nerv Syst* 2013; **29**: 1977–1983.
- Erkek S, Johann PD, Finetti MA, et al. Comprehensive analysis of chromatin states in atypical teratoid/rhabdoid tumor identifies diverging roles for SWI/SNF and polycomb in gene regulation. *Cancer Cell* 2019; **35**: 95–110 e118.
- Chun HE, Lim EL, Heravi-Moussavi A, et al. Genome-wide profiles of extra-cranial malignant rhabdoid tumors reveal heterogeneity and dysregulated developmental pathways. *Cancer Cell* 2016; **29**: 394–406.
- Johann PD, Erkek S, Zapatka M, et al. Atypical teratoid/rhabdoid tumors are comprised of three epigenetic subgroups with distinct enhancer landscapes. *Cancer Cell* 2016; **29**: 379–393.
- Torchia J, Picard D, Lafay-Cousin L, et al. Molecular subgroups of atypical teratoid rhabdoid tumours in children: an integrated genomic and clinicopathological analysis. *Lancet Oncol* 2015; **16**: 569–582.
- Torchia J, Golbourn B, Feng S, et al. Integrated (epi)-genomic analyses identify subgroup-specific therapeutic targets in CNS rhabdoid tumors. *Cancer Cell* 2016; **30**: 891–908.
- Ho B, Johann PD, Grabovska Y, et al. Molecular subgrouping of atypical teratoid/rhabdoid tumors (ATRT) – a reinvestigation and current consensus. *Neuro Oncol* 2020; **22**: 613–624.
- Chun HE, Johann PD, Milne K, et al. Identification and analyses of extra-cranial and cranial rhabdoid tumor molecular subgroups reveal tumors with cytotoxic T cell infiltration. *Cell Rep* 2019; **29**: 2338–2354 e2337.
- Zhang ZK, Davies KP, Allen J, et al. Cell cycle arrest and repression of cyclin D1 transcription by INI1/hSNF5. *Mol Cell Biol* 2002; **22**: 5975–5988.
- Musgrove EA, Caldon CE, Barraclough J, et al. Cyclin D as a therapeutic target in cancer. *Nat Rev Cancer* 2011; **11**: 558–572.
- Tsikitis M, Zhang Z, Edelman W, et al. Genetic ablation of cyclin D1 abrogates genesis of rhabdoid tumors resulting from *Ini1* loss. *Proc Natl Acad Sci U S A* 2005; **102**: 12129–12134.
- McKenna ES, Sansam CG, Cho YJ, et al. Loss of the epigenetic tumor suppressor SNF5 leads to cancer without genomic instability. *Mol Cell Biol* 2008; **28**: 6223–6233.
- Betz BL, Strobeck MW, Reisman DN, et al. Re-expression of hSNF5/INI1/BAF47 in pediatric tumor cells leads to G1 arrest associated with induction of p16ink4a and activation of RB. *Oncogene* 2002; **21**: 5193–5203.
- Doan DN, Veal TM, Yan Z, et al. Loss of the INI1 tumor suppressor does not impair the expression of multiple BRG1-dependent genes or the assembly of SWI/SNF enzymes. *Oncogene* 2004; **23**: 3462–3473.
- Venneti S, Le P, Martinez D, et al. p16^{INK4A} and p14^{ARF} tumor suppressor pathways are deregulated in malignant rhabdoid tumors. *J Neuropathol Exp Neurol* 2011; **70**: 596–609.
- Klein EA, Assoian RK. Transcriptional regulation of the cyclin D1 gene at a glance. *J Cell Sci* 2008; **121**: 3853–3857.
- Alao JP. The regulation of cyclin D1 degradation: roles in cancer development and the potential for therapeutic invention. *Mol Cancer* 2007; **6**: 24.
- Hasselblatt M, Nagel I, Oyen F, et al. *SMARCA4*-mutated atypical teratoid/rhabdoid tumors are associated with inherited germline alterations and poor prognosis. *Acta Neuropathol* 2014; **128**: 453–456.
- Ramos P, Karnezis AN, Craig DW, et al. Small cell carcinoma of the ovary, hypercalcemic type, displays frequent inactivating germline and somatic mutations in *SMARCA4*. *Nat Genet* 2014; **46**: 427–429.
- Witkowski L, Carrot-Zhang J, Albrecht S, et al. Germline and somatic *SMARCA4* mutations characterize small cell carcinoma of the ovary, hypercalcemic type. *Nat Genet* 2014; **46**: 438–443.
- Kupryjańczyk J, Dansonka-Mieszkowska A, Moes-Sosnowska J, et al. Ovarian small cell carcinoma of hypercalcemic type – evidence of germline origin and *SMARCA4* gene inactivation. A pilot study. *Pol J Pathol* 2013; **64**: 238–246.
- Jelinic P, Mueller JJ, Olvera N, et al. Recurrent *SMARCA4* mutations in small cell carcinoma of the ovary. *Nat Genet* 2014; **46**: 424–426.
- Young RH, Oliva E, Scully RE. Small cell carcinoma of the ovary, hypercalcemic type. A clinicopathological analysis of 150 cases. *Am J Surg Pathol* 1994; **18**: 1102–1116.
- Foulkes WD, Clarke BA, Hasselblatt M, et al. No small surprise – small cell carcinoma of the ovary, hypercalcemic type, is a malignant rhabdoid tumour. *J Pathol* 2014; **233**: 209–214.
- Fahiminiya S, Witkowski L, Nadaf J, et al. Molecular analyses reveal close similarities between small cell carcinoma of the ovary, hypercalcemic type and atypical teratoid/rhabdoid tumor. *Oncotarget* 2016; **7**: 1732–1740.
- Xue Y, Meehan B, Fu Z, et al. *SMARCA4* loss is synthetic lethal with CDK4/6 inhibition in non-small cell lung cancer. *Nat Commun* 2019; **10**: 557.
- Xue Y, Meehan B, Macdonald E, et al. CDK4/6 inhibitors target *SMARCA4*-determined cyclin D1 deficiency in hypercalcemic small cell carcinoma of the ovary. *Nat Commun* 2019; **10**: 558.
- O’Leary B, Finn RS, Turner NC. Treating cancer with selective CDK4/6 inhibitors. *Nat Rev* 2016; **13**: 417–430.
- Sherr CJ, Beach D, Shapiro GI. Targeting CDK4 and CDK6: from discovery to therapy. *Cancer Discov* 2016; **6**: 353–367.
- Clark AS, Karasic TB, DeMichele A, et al. Palbociclib (PD0332991) – a selective and potent cyclin-dependent kinase inhibitor: a review of pharmacodynamics and clinical development. *JAMA Oncol* 2016; **2**: 253–260.
- O’Donnell KA, Wentzel EA, Zeller KI, et al. c-Myc-regulated microRNAs modulate E2F1 expression. *Nature* 2005; **435**: 839–843.
- Raab JR, Runge JS, Spear CC, et al. Co-regulation of transcription by BRG1 and BRM, two mutually exclusive SWI/SNF ATPase subunits. *Epigenetics Chromatin* 2017; **10**: 62.
- Magnus N, Garnier D, Meehan B, et al. Tissue factor expression provokes escape from tumor dormancy and leads to genomic alterations. *Proc Natl Acad Sci U S A* 2014; **111**: 3544–3549.
- Venneti S, Garimella MT, Sullivan LM, et al. Evaluation of histone 3 lysine 27 trimethylation (H3K27me3) and enhancer of Zest 2 (EZH2) in pediatric glial and glioneuronal tumors shows decreased

- H3K27me3 in *H3F3A* K27M mutant glioblastomas. *Brain Pathol* 2013; **23**: 558–564.
41. Oruetebarria I, Venturini F, Kekalainen T, *et al.* p16^{INK4a} is required for hSNF5 chromatin remodeler-induced cellular senescence in malignant rhabdoid tumor cells. *J Biol Chem* 2004; **279**: 3807–3816.
 42. Versteeg I, Medjkane S, Rouillard D, *et al.* A key role of the hSNF5/INI1 tumour suppressor in the control of the G1–S transition of the cell cycle. *Oncogene* 2002; **21**: 6403–6412.
 43. Roberts CW, Orkin SH. The SWI/SNF complex – chromatin and cancer. *Nat Rev Cancer* 2004; **4**: 133–142.
 44. Euskirchen GM, Auerbach RK, Davidov E, *et al.* Diverse roles and interactions of the SWI/SNF chromatin remodeling complex revealed using global approaches. *PLoS Genet* 2011; **7**: e1002008.
 45. Yu Z, Wang C, Wang M, *et al.* A cyclin D1/microRNA 17/20 regulatory feedback loop in control of breast cancer cell proliferation. *J Cell Biol* 2008; **182**: 509–517.
 46. Qin X, Wang X, Wang Y, *et al.* MicroRNA-19a mediates the suppressive effect of laminar flow on cyclin D1 expression in human umbilical vein endothelial cells. *Proc Natl Acad Sci U S A* 2010; **107**: 3240–3244.
 47. Trompeter HI, Abbad H, Iwanuk KM, *et al.* MicroRNAs MiR-17, MiR-20a, and MiR-106b act in concert to modulate E2F activity on cell cycle arrest during neuronal lineage differentiation of USSC. *PLoS One* 2011; **6**: e16138.
 48. Zhang Y, Guo X, Li Z, *et al.* A systematic investigation based on microRNA-mediated gene regulatory network reveals that dysregulation of microRNA-19a/Cyclin D1 axis confers an oncogenic potential and a worse prognosis in human hepatocellular carcinoma. *RNA Biol* 2015; **12**: 643–657.
 49. Jonas S, Izaurralde E. Towards a molecular understanding of microRNA-mediated gene silencing. *Nat Rev Genet* 2015; **16**: 421–433.
 50. Mei S, Qin Q, Wu Q, *et al.* Cistrome data browser: a data portal for ChIP-Seq and chromatin accessibility data in human and mouse. *Nucleic Acids Res* 2017; **45**: D658–D662.
 51. You JS, De Carvalho DD, Dai C, *et al.* SNF5 is an essential executor of epigenetic regulation during differentiation. *PLoS Genet* 2013; **9**: e1003459.
 52. Raab JR, Resnick S, Magnuson T. Genome-wide transcriptional regulation mediated by biochemically distinct SWI/SNF complexes. *PLoS Genet* 2015; **11**: e1005748.
 53. Ventura A, Young AG, Winslow MM, *et al.* Targeted deletion reveals essential and overlapping functions of the miR-17~92 family of miRNA clusters. *Cell* 2008; **132**: 875–886.
 54. Olive V, Bennett MJ, Walker JC, *et al.* miR-19 is a key oncogenic component of mir-17-92. *Genes Dev* 2009; **23**: 2839–2849.
 55. Erhard F, Haas J, Lieber D, *et al.* Widespread context dependency of microRNA-mediated regulation. *Genome Res* 2014; **24**: 906–919.
 56. Smith ME, Cimica V, Chinni S, *et al.* Therapeutically targeting cyclin D1 in primary tumors arising from loss of Ini1. *Proc Natl Acad Sci U S A* 2011; **108**: 319–324.
 57. Smith ME, Cimica V, Chinni S, *et al.* Rhabdoid tumor growth is inhibited by flavopiridol. *Clin Cancer Res* 2008; **14**: 523–532.
 58. Mendell JT. miRiad roles for the miR-17-92 cluster in development and disease. *Cell* 2008; **133**: 217–222.
 59. Georger B, Bourdeaut F, DuBois SG, *et al.* A phase I study of the CDK4/6 inhibitor ribociclib (LEE011) in pediatric patients with malignant rhabdoid tumors, neuroblastoma, and other solid tumors. *Clin Cancer Res* 2017; **23**: 2433–2441.
 60. Reddy AT, Strother DR, Judkins AR, *et al.* Efficacy of high-dose chemotherapy and three-dimensional conformal radiation for atypical teratoid/rhabdoid tumor: a report from the Children's Oncology Group trial ACNS0333. *J Clin Oncol* 2020; **38**: 1175–1185.
 61. Hashizume R, Zhang A, Mueller S, *et al.* Inhibition of DNA damage repair by the CDK4/6 inhibitor palbociclib delays irradiated intracranial atypical teratoid rhabdoid tumor and glioblastoma xenograft regrowth. *Neuro Oncol* 2016; **18**: 1519–1528.
 62. Dobin A, Davis CA, Schlesinger F, *et al.* STAR: ultrafast universal RNA-seq aligner. *Bioinformatics* 2013; **29**: 15–21.
 63. Anders S, Pyl PT, Huber W. HTSeq – a Python framework to work with high-throughput sequencing data. *Bioinformatics* 2015; **31**: 166–169.
 64. Love MI, Huber W, Anders S. Moderated estimation of fold change and dispersion for RNA-seq data with DESeq2. *Genome Biol* 2014; **15**: 550.
 65. Subramanian A, Tamayo P, Mootha VK, *et al.* Gene set enrichment analysis: a knowledge-based approach for interpreting genome-wide expression profiles. *Proc Natl Acad Sci U S A* 2005; **102**: 15545–15550.

References 62 - 65 are cited only in the supplementary material.

SUPPLEMENTARY MATERIAL ONLINE

Supplementary materials and methods

Figure S1. SMARCB1 restoration suppresses the growth of ATRT cells

Figure S2. mRNA expression of *CCND1* in ATRT cells with SMARCB1 restoration

Figure S3. *MIR17HG* knockdown in BT16 cells

Figure S4. *miR-17/19a* knockdown in BT12 and CHLA-06 cells

Figure S5. *MIR17HG* knockdown has no clear effect on expression of PTEN and BIM in ATRT cells

Figure S6. *MIR17HG* and *CCND1* mRNA expression in NHA and ATRT cells

Table S1. Genes significantly regulated by SMARCA4 restoration in CHLA-06 and BT-12 cells